

The state of the molecular gas in a luminous starburst/Seyfert 2 galaxy: NGC 1068 revisited

Padeli. P. Papadopoulos¹

Sterrewacht Leiden, P. O. Box 9513, 2300 RA Leiden, The Netherlands

and

E. R. Seaquist

Department of Astronomy, University of Toronto, 60 St. George st. Toronto,
ON M5S-3H8, Canada.

Received _____; accepted _____

¹Department of Astronomy, University of Toronto, 60 St. George st. Toronto,
ON M5S-3H8, Canada.

ABSTRACT

We present fully sampled ^{12}CO , ^{13}CO $J=2-1$, $3-2$ maps of the inner $\sim 1' \times 1'$ region of NGC 1068. We combine these measurements with an existing interferometric map of ^{12}CO $J=1-0$ that includes single dish data and thus contains all the flux present. This allows a reliable estimate of the ^{12}CO ($J=3-2$)/($J=1-0$) ratio at the highest angular resolution currently possible and the use of this sensitive line ratio to probe the physical condition of the molecular gas. We also present two measurements of the faint C^{18}O $J=2-1$ emission which confirm earlier measurements of a high $\text{C}^{18}\text{O}/^{13}\text{CO}$ intensity ratio in this galaxy. The ratios of the ^{12}CO , ^{13}CO isotopes can only be reproduced for small/moderate optical depths of ^{12}CO $J=1-0$ ($\tau \sim 1 - 2$) which is incompatible with the high $\text{C}^{18}\text{O}/^{13}\text{CO}$ ratios observed. A simple two-phase model for the gas can account for all the observed line ratios if the C^{18}O emission and part of the ^{13}CO emission arise in a dense spatially concentrated component, where C^{18}O $J=1-0$ has optical depths of $\tau \gtrsim 1$. The ^{12}CO emission originates from a warmer, diffuse gas phase with $\tau \sim 1 - 2$ for $J=1-0$. The dense gas phase contains the bulk of the molecular gas mass while the diffuse phase may not be virialized leading to an overestimate of molecular gas mass when deduced from the luminosity of the ^{12}CO $J=1-0$ line and a standard galactic conversion factor. This suggests that, since type 2 Seyferts harbor a central starburst more often than type 1, the higher average ^{12}CO $J=1-0$ luminosity of type 2 hinted by earlier studies may simply reflect a difference in molecular gas excitation rather than in gas mass.

Subject headings: galaxies: individual (NGC 1068)—galaxies: Seyfert—galaxies: starburst—ISM: molecules

1. Introduction

Intense central star formation and possibly an Active Galactic Nucleus (AGN) are thought to be the energy sources responsible for the observed large IR luminosities in bright IRAS galaxies (e.g., Telesco 1988; Sanders, Scoville & Soifer 1991) where large amounts of molecular gas are found (Sanders, Scoville & Soifer 1991). An important problem in understanding the energetic phenomena occurring in the nuclear regions of such galaxies is determining the role of the molecular gas in fueling the AGN and/or a central starburst.

Many of the very IR-luminous ($L_{\text{FIR}} > 10^{11} L_{\odot}$) galaxies are found to be strongly interacting or merging systems (Sanders et al. 1988; Lawrence et al. 1989). Strong interactions between two galaxies, at least one of which is gas rich, may foster the rapid accumulation of large amounts of molecular gas in the nuclear regions (Barnes & Hernquist 1991) where they can “ignite” a starburst and “fuel” an AGN. For Seyfert galaxies with more moderate FIR luminosities ($L_{\text{FIR}} \lesssim 10^{11} L_{\odot}$) the picture is less clear. Earlier work by Heckman et al. (1989) suggested that the hosts of type 2 Seyfert nuclei contain, on average, more molecular gas mass and have a larger FIR luminosity and hence higher star forming activity than type 1. More recent studies by Maiolino et al. (1997) of a larger and better defined sample of Seyferts and field spirals confirms the higher FIR luminosities of Seyfert 2’s but casts some doubts on the purported difference in molecular gas mass between these galaxies and Seyfert 1’s, or field spirals. In the same study preliminary evidence points towards bars, interactions and distorted morphologies as being present more frequently in the hosts of type 2 than in type 1 Seyferts. In this case, efficient molecular gas transport towards the nucleus will be present more often in former rather than the latter. Hence, provided that this mechanism remains effective over scales ranging from $L \sim 1$ kpc down to a few parsecs, it can naturally explain why the onset of a central starburst correlates with a higher probability of obscuring the Broad Line Region of the AGN.

Nevertheless such a scenario still cannot explain a larger total molecular gas reservoir in Seyfert 2 with respect to Seyfert 1 galaxies. However, since type 2 are more likely to harbor a central ($\sim 1 - 5$ kpc) starburst than Seyfert 1's (Maiolino 1995), there exists the possibility that any difference in their average ^{12}CO $J=1-0$ luminosities is caused by differences in the average excitation of the molecular gas rather than the total gas mass.

NGC 1068 is the closest and best studied example of a luminous Seyfert 2 galaxy which also harbors an intense starburst in its central ~ 2.5 kpc. It has a large bolometric luminosity of $\sim 3 \times 10^{11} L_\odot$ roughly equally divided between the unresolved AGN and the starburst disk (Telesco et al. 1984). The distribution of molecular gas is characterized by a nuclear concentration within the central 100 pc (Planesas, Scoville & Myers 1991; Helfer & Blitz 1995) where mostly dense gas ($n(\text{H}_2) \sim 10^5 \text{ cm}^{-3}$) resides (Jackson et al. 1993; Tacconi et al. 1994; Helfer & Blitz 1995) and a more extended molecular gas distribution that coincides with the starburst region and consists of two inner spiral arms and a bar (Helfer & Blitz 1995). The nuclear component is thought to contribute to the built-up of an AGN-obscuring molecular torus (Planesas et al. 1991; Cameron et al. 1994; Tacconi et al. 1994). In the present work we use this galaxy as a “laboratory” to study the excitation of the bulk of the molecular gas in the intense starburst environment of the host galaxy of a Seyfert 2 nucleus. To do so we use our fully sampled maps of ^{12}CO , ^{13}CO $J=3-2$, $2-1$ acquired with the James Clerk Maxwell Telescope (JCMT)² in combination with an existing interferometric ^{12}CO $J=1-0$ map (Helfer & Blitz 1995).

Resolution-matched observations of different rotational lines of ^{12}CO and especially ^{13}CO provide an excellent probe of the physical conditions in the bulk of the molecular

²The JCMT is operated by the Joint Astronomy Center in Hilo, Hawaii on behalf of the parent organizations PPARC in the United Kingdom, the National Research Council of Canada and the The Netherlands Organization for Scientific Research.

gas. A ratio like (3–2)/(1–0) can be particularly sensitive to gas excitation conditions since the $J=3$ level lies 32 K above ground versus 5.5 K for $J=1$ while the $J=3–2$ transition has a significantly higher critical density ($n_{\text{cr}} = 4 \times 10^4 \text{ cm}^{-3}$) than the $J=1–0$ transition ($n_{\text{cr}} = 2 \times 10^3 \text{ cm}^{-3}$) in the optically thin regime. Moreover the maps of the rare ^{13}CO isotope allow the study of the molecular gas using less opaque lines than the ones of ^{12}CO and therefore sensitive to the average conditions of a larger fraction of molecular material.

Throughout this study we assume a distance to NGC 1068 of $D=14 \text{ Mpc}$ (Sandage & Tammann 1981, $H_0 = 75 \text{ km s}^{-1}$) for which $1''$ corresponds to 68 pc.

2. OBSERVATIONS

We used the receivers A2, B3i and the newly commissioned receiver B3 on JCMT in several observing runs in order to produce fully sampled maps (Nyquist sampling) of the emission lines ^{12}CO , ^{13}CO $J=3–2$, $2–1$ of the inner $\sim 1' \times 1'$ region of NGC 1068. We also observed the very weak C^{18}O $J=2–1$ transition in two points, the details of all our observations are summarized in Table 1.

EDITOR: PLACE TABLE 1 HERE

The map center was located at $\alpha(\text{B1950}) = 02^{\text{h}} 40^{\text{m}} 07^{\text{s}}.06$, $\delta(\text{B1950}) = -00^{\circ} 13' 31.45''$ and the receiver was tuned to a velocity of $v_{\text{LSR}} = 1125 \text{ km s}^{-1}$. For more efficient mapping of the CO emission, the area mapped was along a rotated grid with $\text{PA} = 40^{\circ}$. The grid-cell is an equilateral triangle with a size of $\Delta\theta_s \sim \theta_{\text{HPBW}}/2$, where θ_{HPBW} is the HPBW of the gaussian beam. This grid provides the optimum coverage of the CO-emitting region of NGC 1068 at a Nyquist sampling and is uniquely determined by the demand of a) a uniform sampling pattern and, b) every sampled point having the maximum number ($N=6$) of the

closest neighboring points at a distance of $\Delta\theta_s$. We performed all our observations using beam switching with a beam throw of $150''$ in azimuth at the recommended rate of 1 Hz and only for the very weak C^{18}O $J=2-1$ the rate was 2 Hz in order to achieve a stable baseline. The pointing and focus were monitored frequently by observing bright quasars, planets and OMC1 (for ^{13}CO $J=3-2$).

We converted the T_A^* temperature scale of the JCMT spectra to the T_{mb} scale by using the relation $T_{\text{mb}} = T_A^*/\eta_{\text{mb}}$. We performed measurements of η_{mb} for all the receivers by observing Saturn (A2, B3i) and Jupiter (B3). We found excellent agreement (within $\sim 10\%$) with the values reported in the JCMT manual (Matthews 1996). The adopted beam efficiencies are $\eta_{\text{mb}}(\text{A2}) = 0.69$, $\eta_{\text{mb}}(\text{B3i}) = 0.55$ and $\eta_{\text{mb}}(\text{B3}) = 0.62$. The error associated with the line intensity measurements was estimated using the relation

$$\left(\frac{\delta T}{T}\right) = \left[\left(\frac{\delta T}{T}\right)_{\text{ther}}^2 + \left(\frac{\delta T}{T}\right)_{\text{calib}}^2 + \left(\frac{\delta T}{T}\right)_{\text{syst}}^2 \right]^{1/2}. \quad (1)$$

The first two terms express the thermal rms error and the stochastic uncertainty of the calibration of the line intensities. The third term is the systematic uncertainty of the assumed telescope efficiency factors. If T is the main beam brightness temperature averaged over N_{ch} channels and N_{bas} is the total number of channels defining a symmetric baseline around the spectral line, then

$$\left(\frac{\delta T}{T}\right)_{\text{ther}} = \frac{\delta T_{\text{ch}}}{T} \left(\frac{N_{\text{bas}} + N_{\text{ch}}}{N_{\text{bas}} N_{\text{ch}}} \right)^{1/2}, \quad (2)$$

where δT_{ch} is the thermal noise per channel.

The calibration uncertainty factor was estimated from the dispersion of the observed intensities of many spectral line standards with high S/N, and it was found to be $\sim 0.10 - 0.15$ for all the observed frequencies. The third factor is ~ 0.10 for all frequencies

(Friberg, Sandell, private communication). Finally we performed an additional check on the overall uncertainty of the line intensities by frequently monitoring the ^{12}CO lines in some standard points of our map. For the weak ^{13}CO lines we monitored the spectrum of OMC1 at $V_{\text{LSR}} = 1125 \text{ km s}^{-1}$ where various bright lines are still present. In all cases we found excellent agreement of the line profiles and a measured dispersion of line intensities consistent with the one estimated from the first two terms of Equation 1.

3. DATA REDUCTION

The JCMT data were reduced using the SPECX reduction package. We smoothed all our spectra to a common velocity resolution of $\Delta V_{\text{chan}} \sim 8 \text{ km s}^{-1}$ and removed linear baselines. In the case of the ^{12}CO $J=3-2$ transition we also removed some bad channels that were present at the high velocity end of the band.

The grid maps were interpolated by convolving them with a gaussian function. For the $J=3-2$ maps the FWHM of the interpolating function used was $\theta_i = 8''$. The interpolated map has effective resolution of $[\theta_i^2 + \theta_{\text{HPBW}}^2(3-2)]^{1/2} = 16''$. For the $J=2-1$ grid maps we used $\theta_i = 11''$ and the effective resolution of the interpolated map is $[\theta_i^2 + \theta_{\text{HPBW}}^2(2-1)]^{1/2} \sim 24''$. The maps were further analyzed with the AIPS reduction package. The task HGEOM was employed to re-grid the JCMT maps in order to re-orient them in an (RA, DEC) grid. A check of the consistency of the interpolation and re-gridding was performed by comparing the area-averaged T_{mb} in individual channel maps between the original grid maps and the final ones used in our analysis. We found good agreement within the thermal rms uncertainties. The maps of the velocity-averaged main beam brightness $\langle T_{\text{mb}} \rangle_{\Delta v}$ for ^{12}CO , ^{13}CO are shown in Figures 1 and 2 for the $J=2-1$ and $3-2$ transitions respectively.

EDITOR: PLACE FIGURE 1 HERE.

EDITOR: PLACE FIGURE 2 HERE.

The ^{12}CO $J=1-0$ map used in our analysis was obtained by Helfer & Blitz (1995) with the Berkeley-Illinois-Maryland Association (BIMA) interferometer and the NRAO 12m telescope. This map is the most suitable one for comparison with our JCMT maps since its combination of interferometer and single dish measurements recovers all the CO flux. The interferometer map has been corrected for primary beam attenuation by assuming a gaussian profile with $\text{HPBW}=100''$. We convolved the ^{12}CO $J=1-0$ channel maps to a spatial resolution of $16''$ and converted the original brightness units (mJy/beam) to the T_{mb} temperature scale in order to compare them to the ^{12}CO $J=3-2$ map. The channel maps and the associated line ratio $r_{32} = (3 - 2)/(1 - 0)$ are shown in Figure 3.

EDITOR: PLACE FIGURE 3 HERE.

The close correspondence of the ^{12}CO $J=3-2$ and the ^{12}CO $J=1-0$ emission in every channel demonstrates that no serious pointing offsets are present between the two maps. The estimated channel-to-channel rms dispersion of the r_{32} ratio is of the order of 10%. This includes only the thermal rms error since the other two sources of error for the JCMT maps (Equation 1) and the systematic calibration uncertainty in the flux conversion factor of the BIMA ^{12}CO $J=1-0$ map are constant across the passband. The largest single source of error is the $\sim 30\%$ flux calibration uncertainty of the ^{12}CO $J=1-0$ BIMA map. This results to a total uncertainty of 35% for the r_{32} ratio.

The C^{18}O $J=2-1$ spectra correspond to a spatial resolution of $\theta_{\text{HPBW}} = 22''$. In order to compare them to the ^{13}CO spectra towards the same locations we used an interpolated ^{13}CO $J=2-1$ map with $\theta_{\text{G}} = 8''$, which gives an effective resolution of $\theta_{\text{i}} = 23''$. The spectra, smoothed to a common frequency resolution of 25 MHz (34 km s^{-1}) are shown in Figure 4.

EDITOR: PLACE FIGURE 4 HERE.

4. RESULTS

The ^{13}CO , ^{12}CO $J=2-1$ and $3-2$ maps (Figures 1, 2) demonstrate that the relative intensities of these two isotopes change significantly across the emitting region. There is a significant increase of the intensity of ^{13}CO relative to ^{12}CO towards the location of the giant molecular gas associations (GMAs) in the southern part of the central starburst region of NGC 1068. These molecular gas concentrations show up in high resolution maps (Planesas, Scoville & Myers 1991; Helfer & Blitz 1995) as high brightness regions with large inferred H_2 surface densities. Especially large variations of $^{12}\text{CO}/^{13}\text{CO}$ are observed for the $J=1-0$ transition (Helfer & Blitz 1995; Papadopoulos, Seaquist & Scoville 1996). Large variations of this ratio have been recently reported by Aalto et al. (1997) in the extreme starburst/merger system Arp 299 where high resolution interferometric measurements indicate changes by a factor of ~ 6 .

The r_{32} ratio also shows a large range of values in the various regions in the inner 3 kpc of NGC 1068 (Fig. 3). The lowest values $r_{32} \sim 0.3 - 0.4$ occur towards the eastern part of the emission while the highest ones $r_{32} \sim 0.6 - 0.8$, towards the western and southwestern part where the bright GMAs are located. Moreover, the ratio r_{21} varies in a similar fashion with a range of $r_{21} \sim 0.6 - 0.7$ and $r_{21} \sim 0.7 - 0.8$ for the eastern and the western/southwestern parts of the emission respectively.

Line ratios as low as $r_{32} \sim 0.3 - 0.4$ characterize the bulk of the relatively cold gas in the Giant Molecular Clouds (GMCs) in the disk of the Galaxy (Sanders et al. 1993). The same is true for $r_{21} \lesssim 0.7$, usually measured in the outer disk of the Galaxy (Hasegawa 1997), or the disks of other galaxies (e.g., Eckart et al. 1990; Eckart et al. 1991). An LTE approximation of such low ratios yields a $T_{\text{kin}} \lesssim 6$ K, comparable to the minimum value of 7 K permitted by cosmic ray heating (Goldsmith & Langer 1978). Then a maximum brightness of ^{12}CO $J=1-0$ would be $T_b \sim 3$ K, much smaller what is usually measured in

NGC 1068 (Planesas, Scoville & Myers 1991), which implies sub-thermal excitation of the J=3–2, 2–1 transitions towards the regions with such low r_{32} and r_{21} ratios.

On the other hand ratios as high as $r_{32} \sim 0.6 - 1$ are measured towards central regions of starbursts (Devereux et al. 1994; Wild et al. 1992) and close to the cores of star forming GMCs like W3 in the Milky Way (e.g., Phillips et al. 1981). A ratio of $r_{21} \sim 0.80 - 1.0$ is found mainly towards the centers of nearby spirals (Braine & Combes 1992), centers of starbursts (e.g., Eckart et al. 1990; Eckart et al. 1991; Wild et al. 1992), close to HII regions and star forming cores in the Galaxy (Hasegawa 1997). In NGC 1068 the largest values ($r_{32} = 0.8$ and $r_{21} = 1$) are observed towards the location of the most massive GMAs identified in the interferometer maps. Under LTE conditions these ratios imply average kinetic temperatures of $T_{\text{kin}} \gtrsim 25$ K. In contrast, the bulk of the molecular gas in the plane of the Milky Way is significantly colder at $T_{\text{kin}} \approx 10$ K (Sanders et al. 1993), undoubtly the result of a more quiescent environment than the central starburst region of NGC 1068.

4.1. The isotope line ratios

As reported previously the value of $^{12}\text{CO}/^{13}\text{CO}$ ratio changes across the central kpc-size starburst region of NGC 1068 with the largest variations measured for the J=1–0 transition. This shows most prominently in high resolution interferometer maps (Papadopoulos et al. 1996) but even in the area-averaged spectra shown in Figure 5.

EDITOR: PLACE FIGURE 5 HERE.

These spectra demonstrate that the ratio $R_{10} = ^{12}\text{CO}/^{13}\text{CO}$ (J=1–0) changes by a factor of ~ 2 along the line profile while variations of R_{21} (J=2–1) and R_{32} (J=3–2) follow in a similar fashion but are significantly less prominent. It is important to note that the

variation of R_{10} across the line profile is not influenced by the systematic uncertainties of the line intensities, since they can only introduce an overall shift of the T_{mb} scale. The line shapes are subject only to the thermal rms error across the bandpass which is of the order of $\sim 10\%$ for the $J=1-0$, and $\sim 15\%$ for the $J=2-1$ and $3-2$ transitions.

The reason for using the OVRO ^{13}CO $J=1-0$ spectrum (Papadopoulos et al. 1996), which does not include single dish data, instead of the one from BIMA/NRAO 12m (Helfer & Blitz 1995) stems from the fact the later has a significantly lower S/N, a result of poor weather during the observations (Helfer, private communication). Nevertheless both data sets exhibit the same basic characteristics. Moreover, the largest variation of R_{10} is found among the low and the high velocity end of the $J=1-0$ line profile, where the addition of the single flux data is not expected to alter the line intensity (Helfer & Blitz 1995).

In the inner kiloparsec-size region of NGC 1068 we find $R_{J+1, J} \gtrsim 10$ ($J=0, 1, 2$) throughout, irrespective of location or averaging scale. For the entire range of the $[^{12}\text{CO}/^{13}\text{CO}]$ abundance values (e.g., Langer & Penzias 1993; Henkel & Mauersberger 1993) such high isotopic ratios correspond to low ^{12}CO optical depths. Assuming LTE and $[^{12}\text{CO}/^{13}\text{CO}] = 40$, a value of $R_{10} \gtrsim 10$ corresponds to a ^{13}CO $J=1-0$ optical depth of $\tau_{10}^{(13)} \lesssim 0.1$, and hence rather high $r_{21}^{(13)} = r_{21}(^{13}\text{CO})$ and $r_{32}^{(13)} = r_{32}(^{13}\text{CO})$ ratios (or equivalently, high R_{21}, R_{32} ratios) with respect to the ones observed. This has been used to support the notion of two-phase gas in starburst centers (Aalto et al. 1995), yet there is still a wide range of *non-LTE* conditions that must be explored before such a conclusion can be reached. We will see that the best evidence for such a state of the molecular gas comes from the C^{18}O $J=1-0$ (Papadopoulos et al. 1996) and $J=2-1$ data (this work).

4.2. The high $\text{C}^{18}\text{O}/^{13}\text{CO}$ ratio

The ratio $R_{21}^{(18)} = \text{C}^{18}\text{O}/^{13}\text{CO}$ $J=2-1$ obtained at the two positions is $R_{21}^{(18)} = 0.26 \pm 0.07$ and $R_{21}^{(18)} = 0.20 \pm 0.06$ (Figure 4). These values, while somewhat lower, are comparable to the average ratio $R_{10}^{(18)} = 0.3 \pm 0.1$ found from high resolution OVRO maps (Papadopoulos et al. 1996) for the $J=1-0$ transition. Moreover, these maps also show that the C^{18}O emission does not smoothly trace ^{13}CO in the various GMAs and varies drastically from one location to the next with values as high as $R_{10}^{(18)} \sim 0.65$. This is significantly higher than the abundance ratio $[\text{C}^{18}\text{O}/^{13}\text{CO}] = 0.12 - 0.14$ inferred for the Milky Way from various studies (e.g., Wannier 1980; Henkel & Mauersberger 1993; Langer & Penzias 1993). Ratios $R_{10}^{(18)} \gtrsim 0.2$ are also found in several central starbursts of galaxies (e.g., Sage, Mauersberger, & Henkel 1991; Casoli, Durpaz, & Combes 1992; Henkel & Mauersberger 1993).

While it is possible that an enhancement of the $[\text{C}^{18}\text{O}/^{13}\text{CO}]$ abundance can occur in starburst environments (Henkel & Mauersberger 1993) and hence play a role in the observed high values of $R_{10}^{(18)}$ and $R_{21}^{(18)}$, it is very unlikely that it can be solely responsible for the high $R_{10}^{(18)}$ values observed in individual GMAs (Papadopoulos et al. 1996). Furthermore, the large spatial variations of the $R_{10}^{(18)}$ ratio over scales of ~ 400 pc are difficult to attribute solely to a varying $[\text{C}^{18}\text{O}/^{13}\text{CO}]$ abundance because the mixing of interstellar gas is expected to be effective enough to homogenize the isotope ratios over similar or larger scales, even during an ongoing burst of star formation (Henkel & Mauersberger 1993).

Thus, it seems more likely that the optical depth of the rare isotopes is not negligible. For $R_{10}^{(18)} \gtrsim 0.20$, the optical depth of ^{13}CO $J=1-0$ is $\tau_{10}^{(13)} \gtrsim 1.5$ (LTE assumed), which directly contradicts the general conclusion reached earlier from the R_{10} ratio which yields $\tau_{10}^{(13)} \lesssim 0.1$. This constitutes the strongest evidence that ^{12}CO , ^{13}CO and C^{18}O cannot be all tracing the same phase of the molecular gas.

5. DISCUSSION

Line ratios of CO and its isotopes as inputs to a radiative transfer model that solves the rate equations for the various rotational levels are useful probes of the physical conditions of the molecular gas. Obviously the larger the number of the input ratios the better the constraints on the gas properties. The various spectral lines for NGC 1068 have been observed at very different angular resolutions with the lowest one ($\theta_{\text{HPBW}} \sim 24''$ for $J=2-1$) being comparable to the source size. Hence, using the spatially-averaged spectra over the entire CO emitting area ($\sim 1' \times 1'$) allows the estimate of all the line ratios for that area and thus offers the maximum number of inputs that can be used to constrain the physical properties of the molecular gas. These line ratios are tabulated in Table 2.

EDITOR: PLACE TABLE 2 HERE

For the modeling of the molecular gas properties we used a Large Velocity Gradient (LVG) code. We searched an extensive grid of LVG models with a parameter range of $T_{\text{kin}} = 10 - 120$ K ($\Delta T_{\text{kin}} = 2$ K), $n(H_2) = (0.1 - 10^4) \times 10^3$ cm $^{-3}$ ($\Delta \log n(H_2) = 0.5$) and, $\Lambda = X/(dV/dr) = (0.1 - 10^2) \times 10^{-6}$ (km s $^{-1}$ pc $^{-1}$) $^{-1}$ ($\Delta \log \Lambda = 0.5$), where $X = [^{12}\text{CO}/H_2]$ and dV/dr is the velocity gradient for the “average” molecular cloud. We assumed an abundance ratio of $[^{12}\text{CO}/^{13}\text{CO}] = 40$ since studies of the Milky Way (Langer & Penzias 1993) and central regions of starburst galaxies (Henkel et al. 1993; Henkel & Mauersberger 1993) show this value to be a suitable average of the abundances observed towards galactic centers. The abundance of $[C^{18}\text{O}/^{13}\text{CO}] = 0.15$ is derived from $[^{12}\text{CO}/^{13}\text{CO}] = 40$ and $[^{12}\text{CO}/C^{18}\text{O}] = 250$, which is the highest such value derived for molecular clouds in the Milky Way (Wannier 1980), and was measured towards its center. We examine the entire grid of the LVG models for the values of r_{21} , r_{32} that correspond to 0%, -30% and $+30\%$ offset in the BIMA ^{12}CO $J=1-0$ intensity. The best fit is found for the highest r_{21} , r_{32} ratios

which correspond to the 30% reduction in the flux density of the ^{12}CO $J=1-0$ map.

Apart from giving the best fit, such an offset of the ^{12}CO $J=1-0$ intensity observed by BIMA seem to be corroborated by single dish measurements reported by Maiolino et al. (1997) and Kaneko et al. (1989). The first used the NRAO 12m to obtain a velocity-integrated main beam brightness for the inner $55'' \times 55''$ of NGC 1068 which is $I = (90 \pm 13)\text{K km s}^{-1}$, while the latter used the NRO 45m telescope to map a similar area and found $I = (83 \pm 17)\text{K km s}^{-1}$. These values were obtained from their data after converting the T_R^* (NRAO 12m) and T_A^* (NRO 45m) temperature scales to T_{mb} . The integrated flux found over the same region from the BIMA map is $I = (131 \pm 40)\text{K kms}^{-1}$. Clearly only a large offset of $\approx -30\%$ can bring the BIMA value in agreement with the other two. Moreover, adopting such an offset yields $r_{21} = 0.97$, which in much better agreement with the value $r_{21} = 1.1$ reported by Braine & Combes (1992) over the same angular size.

The conditions corresponding to the best fit are $T_{\text{kin}} = 20 \text{ K}$, $n(\text{H}_2) = 10^4 \text{ cm}^{-3}$ and $\Lambda = 10^{-6} (\text{km s}^{-1} \text{ pc}^{-1})^{-1}$. It is interesting to note that Thronson et al (1987) using mm/sub-mm continuum measurements deduce a dust temperature of $T=20 \text{ K}$ for the inner $55''$ of this galaxy, which is similar to the gas temperatures we find from the LVG fits. This is expected for well mixed gas and dust where the ^{12}CO , ^{13}CO lines trace the same “average” conditions as the mm/sub-mm emission originating from dust.

As expected from our previous discussion, the best LVG model cannot reproduce the observed high $\text{C}^{18}\text{O}/^{13}\text{CO}$ line ratios, since the deduced optical depth of the ^{12}CO $J=1-0$ transition is $\tau_{10} \sim 1 - 2$. In this case ^{13}CO , C^{18}O are very optically thin and the ratio of their intensities is equal to their assumed relative abundance. The moderate optical depth of the ^{12}CO $J=1-0$ transition was suggested by Aalto et al. (1995) as being one of the characteristics of a second, more diffuse and warm gas phase that surrounds a dense and more spatially concentrated one in the nuclear regions of starbursts (see also Wall et

al. 1993 for earlier work on spirals). This would naturally explain why both the average brightness of the ^{12}CO $J=1-0$ transition as well as the R_{10} line ratio are more sensitive functions of velocity (and therefore of location within the galaxy) than the $J=2-1$, $3-2$ transitions (Figure 5) and the R_{21} , R_{32} ratios respectively.

For $T_{\text{kin}} \geq 20$ K it is $2.7\tau_{10} \leq \tau_{21} \leq 4\tau_{10}$ and $3\tau_{10} \leq \tau_{32} \leq 9\tau_{10}$ (LTE), hence a moderate $\tau_{10} \sim 1 - 2$ corresponds to $\tau_{J+1, J} \sim 3 - 6$ ($J=1,2$) or higher. This range of τ_{10} values allows the ^{12}CO $J=1-0$ transition to be significantly more sensitive than the $J=2-1$ and $J=3-2$ to variations of gas column density and excitation conditions. Higher values $\tau_{10}(> 2)$ would render all three transitions optically thick and thermalized even at moderate/low ($n(\text{H}_2) \lesssim 10^3$ cm $^{-3}$) gas densities because of radiative trapping, and hence they would be equally “insensitive” to the conditions of the molecular gas except the kinetic temperature. On the other hand, significantly lower values $\tau_{10}(\lesssim 0.1)$ yield small/moderate optical depths for all three transitions and not just $J=1-0$. Hence they will all be sensitive to the gas excitation conditions and their intensities and $R_{J+1, J}$ line ratios will vary strongly along the line profile, reflecting the changing excitation conditions in the inner region of NGC 1068.

An important consequence of the moderate ^{12}CO $J=1-0$ and the correspondingly small (< 0.1) ^{13}CO $J=1-0$ optical depths is that the latter transition can be slightly super-thermally excited (Goldsmith 1972; de Jong et al. 1975; Leung & Liszt 1976). Indeed for the best LVG solution it is $T_{\text{ex}}(1 - 0) > T_{\text{kin}}$ for ^{13}CO . In this case the sensitivity of R_{10} to the excitation conditions with respect to the R_{21} and R_{32} ratios becomes more pronounced while $r_{21} \sim 0.8 - 1.0$, and $r_{21}^{(13)} \lesssim 1.3$ can still be fitted with a single gas phase of small/moderate ^{12}CO $J=1-0$ optical depth ($R_{10} \gtrsim 10$). Later we will see that this property of the ^{13}CO $J=1-0$ transition remains as one the characteristics of the diffuse gas phase in a two-component gas model.

5.1. The heterogeneous gas in NGC 1068

The inability of a single gas phase to account for the line ratios of the ^{12}CO , ^{13}CO and C^{18}O isotopes in the starburst region of NGC 1068 suggests at least two distinct phases. One phase dominating the ^{12}CO while the other is responsible for most of the C^{18}O emission, and with the ^{13}CO having contributions from both.

The notion of a two-component or generally multi-component molecular gas phase seems trivial in the face of numerous studies of the Milky Way and other galaxies that reveal a large range of temperatures $T_{\text{kin}}(\sim 10 - 100\text{K})$ and densities $n(\text{H}_2)(\sim 10^2 - 10^8 \text{ cm}^{-3})$ for the molecular gas. This notion is indeed not particularly useful unless one includes the spatial scale involved. Examination of the physical conditions of the molecular gas on scales of $L \lesssim 1 - 50 \text{ pc}$ is bound to yield a very different picture depending on whether one looks at Orion-type molecular clouds that harbor ongoing star formation or more quiescent ones. Averaging over much larger ($L \gtrsim 0.5 \text{ kpc}$) scales “smoothes” out the local density and temperature irregularities to a degree that a narrow range of temperatures and densities, deduced from molecular line spectroscopy, can fit the observed line ratios.

It is when such “averaging” fails to converge towards a single narrow set of physical conditions that the notion of more than one molecular gas components becomes meaningful and necessary.

Numerous studies of molecular gas in other galaxies (e.g., Knapp et al. 1980; Wall & Jaffe 1990; Eckart et al. 1991; Braine & Combes 1992; Aalto et al. 1995) have demonstrated a broad differentiation of molecular gas properties with warm ($T_{\text{kin}} \gtrsim 20 \text{ K}$) and dense gas ($n(\text{H}_2) \gtrsim 10^4 \text{ cm}^{-3}$) lying in the inner $\sim 0.5 - 1 \text{ kpc}$, while colder ($T_{\text{kin}} \lesssim 10 \text{ K}$), less dense ($n(\text{H}_2) \lesssim 10^3 \text{ cm}^{-3}$) gas is located further out in the disk. A similar differentiation seems to be in place in the Milky Way (e.g., Bally et al. 1988; Stark et al. 1989, 1991; Binney et al. 1991; Spergel & Blitz 1992). The properties of the molecular clouds in galactic

disks seem to be easily described by a single set of molecular gas properties or equivalently the “averaging” of those properties over scales of $L \gtrsim 0.5$ kpc converges to single type of “average” cloud.

This does not seem to be the case for the molecular gas lying in the central galactic regions. Several studies (e.g., Wall & Jaffe 1990; Eckart et al. 1990; Wall et al. 1993; Aalto et al. 1995) indicate that even when averaged over $\sim 0.5 - 1$ kpc, the line emission of the various trace molecules does not point towards a single gas phase but at least two. For starburst centers this “differentiation” of the molecular gas seems to become more acute (Aalto et al. 1995) and is thought to be driven by a variety of mechanisms, namely an intense UV field, large turbulent linewidths, tidal forces and cloud-cloud collisions. In this picture one phase consists of warm and diffuse and low-density molecular gas originating from the heated and disrupted outer envelopes of molecular clouds while the other one consists of the more “protected” interiors of such clouds where the gas is denser and colder.

5.2. A two-phase model for NGC 1068

The wealth of molecular line data gathered for the central starburst region of NGC 1068 allows for another rigorous test of the aforementioned ideas and a better determination of the properties of the two gas phases.

We denote as (B) a dense, concentrated gas phase where ^{13}CO and even C^{18}O may have substantial optical depths and as (A) a diffuse phase where $\tau_{10} \sim 1 - 2$ for ^{12}CO $J=1-0$. Then all the observed line ratios can be expressed as a weighted mean of the ratios of these two phases. Hence the $R_{10}^{(18)}$ line ratio can be expressed as follows:

$$R_{10}^{(18)} = \frac{R_{10}^{(18)}(\text{A}) + [f_c \rho_{13}] R_{10}^{(18)}(\text{B})}{1 + [f_c \rho_{13}]}, \quad (3)$$

where f_c is the filling factor of phase (B) relative to phase (A) and $\rho_{13} = T_R(B)/T_R(A)$ is the ratio of the ^{13}CO $J=1-0$ brightness temperature for the two gas phases.

In phase (A) both ^{13}CO and C^{18}O isotopes are optically thin (so there is little radiative trapping), and since they have the same collisional excitation coefficients and are influenced by the same background radiation field it is $R_{10}^{(18)}(A) = [\text{C}^{18}\text{O}/^{13}\text{CO}]$. Assuming the highest such abundance, measured towards the central regions of the Milky Way (e.g., Wannier 1980; Henkel & Mauersberger 1993; Langer & Penzias 1993), means $R_{10}^{(18)}(A) = 0.15$. Hence, R_{10} can be expressed as

$$R_{10} = \frac{R_{10}(A) + [f_c \rho_{13}] R_{10}(B)}{1 + [f_c \rho_{13}]} \quad (4)$$

The rest of the line ratios $r_{J+1, J}$ and $r_{J+1, J}^{(13)}$ ($J=1, 2$) for ^{12}CO and ^{13}CO respectively can be expressed as follows:

$$r_{J+1, J} = \frac{r_{J+1, J}(A) + [f_c \rho_{12}] r_{J+1, J}(B)}{1 + [f_c \rho_{12}]} \quad (5)$$

$$r_{J+1, J}^{(13)} = \frac{r_{J+1, J}^{(13)}(A) + [f_c \rho_{13}] r_{J+1, J}^{(13)}(B)}{1 + [f_c \rho_{13}]} \quad (6)$$

where $\rho_{12} = T_R(B)/T_R(A)$ denotes the brightness temperature ratio of ^{12}CO $J=1-0$ for the two gas phases. The two factors ρ_{13} and ρ_{12} are related by the simple relation

$$\rho_{12} = \left[\frac{R_{10}(B)}{R_{10}(A)} \right] \rho_{13} \quad (7)$$

We find that the range of the observed line ratios can be reproduced only when $f_c \rho_{13} \lesssim 1$ and $f_c \rho_{12} \ll 1$. The latter yields $r_{21} \approx r_{21}(A)$ and $r_{32} \approx r_{32}(A)$ (Equation 5), i.e., these ratios are dominated by the diffuse phase (A). The C^{18}O $J=1-0$ optical depth for

phase (B) is found to be $\tau_{10}^{(18)} \sim 1$ and hence ^{13}CO and ^{12}CO in this phase are optically thick. Radiative trapping is then enhanced and can thermalize the $J \leq 3$, transitions of ^{12}CO at densities of $n(\text{H}_2) \sim 10^2 \text{ cm}^{-3}$, and ^{13}CO at $n(\text{H}_2) \sim 10^3 \text{ cm}^{-3}$. non-LTE effects are expected to be important for the ^{13}CO , C^{18}O transitions arising in the diffuse phase (A).

In this simple model we assume LTE excitation of the ^{12}CO , ^{13}CO $J=1-0$, $2-1$, $3-2$ and C^{18}O $J=1-0$ transitions for the more spatially concentrated gas phase (B), while making no such assumption for the “envelope”, diffuse gas phase (A). The deduced line ratios for the latter are analyzed using LVG modeling with the same parameter space and abundance ratios as in our previous single-phase LVG analysis. A good solution for phase (A) is found only for $r_{21} = 0.97$, $r_{32} = 0.74$, corresponding to a -30% offset in the BIMA ^{12}CO $J=1-0$ intensity. The results for both gas phases are summarized in Table 3.

EDITOR: PLACE TABLE 3 HERE

5.3. The diffuse gas phase

From Table 3 we see that this gas phase is characterized by small/moderate optical ^{12}CO $J=1-0$ depths of $\tau_{10} \lesssim 1$, relatively low density $n(\text{H}_2) \sim 10^3 \text{ cm}^{-3}$ and probably higher kinetic temperatures than the denser and optically thick phase (B). The ^{13}CO $J=1-0$ transition is now significantly super-thermal, which is responsible for the high $R_{10} = 17$ and moderate $r_{21} \sim 1$ and $r_{21}^{(13)} \sim 1.4$ ratios. This non-LTE effect can occur for a wide range of physical conditions as long as $T_{\text{kin}} \gtrsim 20 \text{ K}$, $n(\text{H}_2) \gtrsim 2 \times 10^3 \text{ cm}^{-3}$ and $\tau_{10}^{(13)} \lesssim 0.1$ (Leung & Liszt 1976). Moreover, the higher the T_{kin} the larger the density regime over which superthermality occurs, e.g., for $T_{\text{kin}} = 60 \text{ K}$ and $\Lambda \sim 10^{-5} (\text{km s}^{-1} \text{ pc}^{-1})^{-1}$ the density range is $n(\text{H}_2) \sim 10^3 - 10^5 \text{ cm}^{-3}$. This includes densities well past the thermalization density of the $J=1-0$ transition ($\sim 2 \times 10^3 \text{ cm}^{-3}$).

These conditions are more likely to be found in starburst environments rather than quiescent ones. There the intense UV radiation and the turbulent motions present will heat and disrupt the molecular clouds and thus create the warm diffuse gas phase where ^{13}CO $J=1-0$ may become super-thermally excited. The line ratios are then sensitive to $(n(\text{H}_2), \Lambda)$ but they generally satisfy $r_{21} \sim 0.8 - 1.1$, $r_{21}^{(13)} \sim 1.2 - 2.2$ and $R_{10} \gtrsim 10$, which contains the range of the values found for these ratios by Aalto et al. (1995) for starbursts.

The high value of the R_{32} ratio for phase (A) (Table 3) significantly restricts the LVG parameter space. This stems from the fact that the conditions for superthermality are bounded by the conditions needed to keep a low τ_{32} (and hence a high R_{32}) which call for a low excitation of the $J=3$ level, i.e., $n(\text{H}_2) < 4 \times 10^4 \text{ cm}^{-3}$ and/or $T_{\text{kin}} < 30 \text{ K}$. However, in a starburst environment a wide range of kinetic temperatures $T_{\text{kin}} (\gtrsim 30) \text{ K}$ can be expected, especially for the “exposed” molecular gas in the outer areas of molecular clouds (Aalto et al. 1995). Hence the aforementioned restrictions to the excitation conditions of the diffuse gas phase become mainly restrictions on its density, namely $10^3 \text{ cm}^{-3} \lesssim n(\text{H}_2) \lesssim 10^4 \text{ cm}^{-3}$.

5.3.1. Gas kinematics and the range of dV/dr

The other important characteristic of the diffuse gas phase is that is probably not virialized. This can be viewed as a direct result of the various mechanisms that create this phase by disrupting initially denser and more compact molecular clouds. After the “envelope” gas phase is created the energetic environment in which it resides may not allow it to settle to self-gravitating structures. Its prevailing kinematic state is important since the velocity-integrated luminosity of ^{12}CO $J=1-0$ is routinely used as an indicator of gas mass in galaxies with one of the key assumptions (among others) being that molecular gas consists of an ensemble of virialized clouds, hence linewidth reflects mass. For ^{12}CO emission dominated by non-virialized diffuse gas this will clearly overestimate the gas mass.

The LVG approximation is valid when the linewidth Δv of the average cloud is larger than the thermal one, i.e., $\Delta v \gg \Delta v_{\text{th}}$. For temperatures of $T_{\text{kin}} \sim 10 - 50$ K the thermal linewidth is $\Delta v_{\text{th}} = 0.1 - 0.2$ km s $^{-1}$. Hence LVG approximation is expected to be valid for linewidths of the order of $\Delta v \gtrsim 10 \times \Delta v_{\text{th}} = 1 - 2$ km s $^{-1}$, which is what is usually observed in individual molecular clouds. An upper limit to the linewidth of such clouds is set by the fact that their individual linewidths cannot be larger than the observed ones in extragalactic systems, which consist of many molecular clouds. For a typical extragalactic linewidth of $\Delta v_G = 300$ km s $^{-1}$ consisting of the linewidths of at least ~ 10 clouds, the maximum linewidth is $\Delta v_{\text{max}} = 0.1 \times \Delta v_G = 30$ km s $^{-1}$. This is a rather generous upper limit since the velocity dispersion seen in large individual Galactic GMCs is of the order of $\Delta v = 3 - 8$ km s $^{-1}$ (Scoville & Good 1989). For a cloud size of $L \sim 0.5 - 50$ pc, the extreme velocity range of $\sim 2 - 30$ km s $^{-1}$ yields a maximum range of $dV/dr \sim (0.04 - 60)$ km s $^{-1}$ pc $^{-1}$ for the average velocity gradient per cloud.

If the “average” cloud is virialized then, for a given average gas density, the expected range for dV/dr is significantly narrower. For a spherical cloud of radius R the virial theorem gives:

$$\left(\frac{dV}{dr} \right)_{\text{VIR}} \approx \frac{\delta v_{\text{vir}}}{2R} = \left(\alpha \frac{\pi G \mu}{3} \right)^{1/2} \langle n \rangle^{1/2}, \quad (8)$$

where μ is the mean mass per particle and $\langle n \rangle$ is the mean number density of the cloud. The factor $\alpha \sim 0.5 - 2.5$ depends primarily on the assumed density profile (see Bryant & Scoville 1996). Expressing the last result in astrophysical units gives

$$\left(\frac{dV}{dr} \right)_{\text{VIR}} \approx 0.65 \alpha^{1/2} \left(\frac{\langle n \rangle}{10^3 \text{cm}^{-3}} \right)^{1/2} \text{km s}^{-1} \text{pc}^{-1}. \quad (9)$$

For NGC 1068, the best LVG solution for phase (A) gives (Table 3) $\langle n \rangle = 3 \times 10^3$ cm $^{-3}$,

so for the largest reasonable value of $\alpha = 2.5$ we estimate $(dV/dr)_{VIR} \sim 2 \text{ km s}^{-1} \text{ pc}^{-1}$. The same model also gives $\Lambda = 3 \times 10^{-6} (\text{km s}^{-1} \text{ pc}^{-1})^{-1}$. For $[\text{^{12}CO}/\text{H}_2] = 10^{-4}$ this yields $dV/dr = 33 \text{ km s}^{-1} \text{ pc}^{-1}$, which is ~ 17 times larger than the virial value. Hence, unless the $[\text{^{12}CO}/\text{H}_2]$ abundance is significantly lower in the diffuse phase, such a large value of dV/dr suggests that this phase is not virialized. A similar situation is found for the starbursting center of IC 342 by Irwin & Avery 1992, which they interpret in terms of a significantly lower $[\text{^{12}CO}/\text{H}_2]$ abundance rather than in terms of non-virialized gas. In Ultraluminous Infrared Galaxies, such a gas phase seems to be filling the entire intercloud medium (Solomon et al. 1997) in the inner few hundred parsecs.

In all these cases the ^{12}CO linewidth will have other significant contributions besides the gravitational potential of the gas itself, namely pressure, stellar and other CO-dark mass (Downes et al. 1993) and the general potential of the galaxy (Solomon et al. 1997).

5.4. The dense gas phase

A lower limit for the gas density of phase (B) can be deduced from the information in Table 3 and the fact that LTE provides a good description of the excitation of the gas in this phase. The optical depth of the C^{18}O $J=1-0$ transition can be expressed as follows

$$\tau_{10}^{(18)} = 1.23 \times 10^4 \left(\frac{1 - e^{-5.26/T_{\text{kin}}}}{T_{\text{kin}}} \right) \left[\frac{\text{C}^{18}\text{O}}{\text{H}_2} \right] n(\text{H}_2) \left(\frac{dV}{dr} \right)^{-1}, \quad (10)$$

where T_{kin} is the kinetic temperature of the gas in (B) phase.

Assuming that the “average” cloud of this gas phase is a virialized structure means that dV/dr is given by Equation 9, so for an abundance $[\text{^{12}CO}/\text{H}_2] = 10^{-4}$ we get

$$n(H_2) = 2.78 \times 10^{-4} \alpha \left(\frac{T_{\text{kin}}}{1 - e^{-5.26/T_{\text{kin}}}} \right)^2 \left[\frac{^{12}\text{CO}}{^{18}\text{O}} \right]^2 (\tau_{10}^{(18)})^2. \quad (11)$$

A temperature of $T_{\text{kin}} = 10$ K and an optical depth of $\tau_{10}^{(18)} = 0.7$ are the minimum values characterizing phase (B). These values and an abundance of $[^{12}\text{CO}/^{18}\text{O}] = [^{12}\text{CO}/^{13}\text{CO}] \times [^{13}\text{CO}/^{18}\text{O}] = 40 \times 1/0.15 \approx 267$ yield a gas density of $n(H_2) \approx 10^4 \text{ cm}^{-3}$ ($\alpha = 1.5$). This is a minimum value since T_{kin} can attain significantly larger values (Table 3) which would yield larger values of $n(H_2)$, e.g., for $T_{\text{kin}} = 20$ K and $\tau_{10}^{(18)} = 1.1$ it is $n(H_2) \approx 3 \times 10^5 \text{ cm}^{-3}$. Such densities are comparable to the average densities found in the cores of molecular clouds like Orion, M 17 and Cepheus by Bergin et al. (1996) which also find good agreement between the virial masses and the ones deduced from ^{18}O observations (Goldsmith et al. 1997). Situations where even the rare ^{18}O isotope may have moderate optical depth and is associated with high density molecular gas are known. In these cases ^{18}O shows good kinematic and spatial correspondence with much higher dipole moment molecules like HC_3N (Bergin et al. 1996) and NH_3 (Fuente 1993). Similarly high densities but with higher average temperatures are found also towards the Galactic Center region (Guesten 1989).

The large abundance ratio $[^{12}\text{CO}/^{18}\text{O}]$ plays a crucial role in making these two isotopes suitable for broadly tracing the two gas phases described previously. Indeed, while it is frequently said that molecules with high dipole moments (e.g., CS, HCN) are needed in order to trace high density gas, to a certain extent, rare CO isotopes can do the same. This happens because unlike the high density tracing molecules, ^{12}CO has an abundance high enough for moderate/high optical depth to arise in the general conditions of the ISM. Most of the emission of a transition arises in regions where $\tau \gtrsim 1$ and the transition is thermalized. Thus ^{12}CO $J=1-0$ can trace a diffuse gas phase since, for $\tau_{10} \sim 1 - 10$, radiative trapping will thermalize this transition at $n_A(H_2) = n_{\text{crit}} \times (1 - e^{-\tau_{10}})/\tau_{10} \approx 10^2 - 10^3 \text{ cm}^{-3}$,

where n_{crit} is the critical density of the $J=1-0$ transition. On the other hand, assuming uniform gas excitation, the less abundant isotope C^{18}O with $[\text{^{12}\text{CO}}/\text{C}^{18}\text{O}] = 250 - 500$ (Wannier 1980), will attain an optical depth of $\tau_{10} \sim 1$ in regions with densities of $n_B(\text{H}_2) \sim (250 - 500) \times n_A(\text{H}_2) \gtrsim 2 \times 10^4 \text{ cm}^{-3}$.

5.5. The changing physical conditions of the gas

The different angular resolution of the maps of the various CO transitions prevent us from using all the observed line ratios to study the molecular gas within the starburst region of NGC 1068 at a common, high angular resolution. Nevertheless, the wide range of physical conditions can be revealed from the r_{32} and R_{10} ratios alone and simple one-phase LVG modeling. Apart from the fact that both these ratios are sensitive to gas excitation they can be estimated at the highest possible resolutions, and hence because of less spatial smoothing they can be sensitive to a wider range of physical conditions. For $R_{10} \gtrsim 10$ ($\langle R_{10} \rangle = 14$) the range of r_{32} ($\sim 0.4 - 0.8$) corresponds to $T_{\text{kin}} \geq 20\text{K}$, $n(\text{H}_2) = 10^3 - 10^4 \text{ cm}^{-3}$ and $\Lambda = 10^{-6} - 10^{-5} (\text{km s}^{-1} \text{ pc}^{-1})^{-1}$. For $r_{32} = 0.57 - 1.1$ (-30% offset for ^{12}CO $J=1-0$) this parameter space becomes even wider. In all cases we find the most dense gas inferred for the large GMAs in the western part of the central emission.

Using all the global line ratios and our simple two-phase model confirms the results of the one-phase LVG analysis. For the “low-velocity” CO emission ($V_{\text{LSR}} \sim 980 - 1050 \text{ km s}^{-1}$) corresponding to GMAs in the easternmost part of the central region (Helfer & Blitz 1995) we find negligible contribution of the dense gas phase (B) to the ^{12}CO and the ^{13}CO emission, and the diffuse phase (A) seems to be the dominant component. For the “high-velocity” CO emission ($V_{\text{LSR}} \sim 1200 - 1280 \text{ km s}^{-1}$) originating from the GMAs located in the westernmost part there is a significant contribution from the dense and optically thick gas phase (B). This picture is further supported by a sensitive map of the

HCN J=1–0 which traces dense gas made with the IRAM interferometer (Tacconi et al. 1994) at a resolution of $\sim 4'' \times 3''$. This map shows that, apart from the Seyfert nucleus itself, the brightest HCN emission originates from the western part of the inner kpc-size region of NGC 1068 and is most prominent towards the location of the massive GMA at $(\Delta\alpha, \Delta\delta) \approx (-8'', -15'')$ from the center.

Our study lacks sufficient angular resolution to shed more light to the physical conditions of the nuclear gas ($L \lesssim 100$ pc), where warm ($T_{\text{kin}} \gtrsim 70$ K) and dense ($n(H_2) \sim 10^5$ cm $^{-3}$) gas dominates (Tacconi et al. 1994). As we discussed earlier, even the r_{32} ratio at $\sim 16''$, is dominated by the extended CO emission from the GMAs throughout.

5.6. Molecular gas mass in NGC 1068

The most common method used to find molecular gas mass in extragalactic systems relies on the so-called standard galactic conversion factor X_G which converts the luminosity of the ^{12}CO J=1–0 line to gas mass, namely

$$X_G = \frac{M(H_2)}{L_{\text{CO}}} = 5.0 \text{ M}_\odot \text{ (km s}^{-1} \text{ pc}^2\text{)}^{-1}, \quad (12)$$

with its numerical value adopted from Solomon & Barett (1991). The ^{12}CO J=1–0 luminosity L_{CO} is estimated from

$$L_{\text{CO}} = A_s \int_{\Delta v} \int_{A_s} T_b(a, v) \text{ d}a \text{ d}v = \Omega_c D^2 \int_{\Delta v} T_b^{(a)}(v) \text{ d}v, \quad (13)$$

where $T_b^{(a)}(v)$ is the area-averaged spectrum (see Figure 5) and D the distance to the galaxy.

The velocity-integrated brightness of ^{12}CO J=1–0 from the Kaneko et al. (1989), Maiolino et al. (1997) and our measurement (scaled by –30%) give an average of

$\langle I \rangle = 88 \text{ K km s}^{-1}$, over an area of $\sim 1' \times 1'$. Using X_G then gives $M(H_2) \approx 6 \times 10^9 M_\odot$.

Under certain assumptions and taking into account only differences in average density $\langle n(H_2) \rangle$ and ^{12}CO $J=1-0$ brightness temperature $\langle T_b \rangle$ (see Bryant & Scoville 1996 for a more complete treatment), the conversion factor X can be expressed as follows (e.g Radford et al. 1991)

$$X = 2.1 \frac{\sqrt{\langle n(H_2) \rangle}}{\langle T_b \rangle}. \quad (14)$$

From our single-phase LVG analysis we find that $X/X_G \approx 1 - 3$, which can yield gas mass estimates as high as $M(H_2) \approx 1.8 \times 10^{10} M_\odot$.

Several studies (Dickman et al. 1986; Maloney & Black 1988; Bryant & Scoville 1996) attempt to quantify the effects of the molecular gas environment on the value of X , especially when the ^{12}CO emission is optically thick. These studies indicate that, when a standard galactic conversion factor is used, the presence of a non-virialized gas component will result to an overestimate of gas mass, while significant shadowing of molecular clouds in spatial and/or velocity space to an underestimate. Except when the angular resolution is high enough to resolve individual clouds, cloud-cloud shadowing may be important only towards very quiescent cloud environments unlike the ones expected in a central starburst. Therefore the sole most important factor affecting X is the presence of a non-virialized gas component where molecular cloud linewidths are no longer good mass indicators.

A different method is to use rare isotopes of CO like ^{13}CO or C^{18}O to deduce molecular gas mass. The main assumption here is that these isotopes have small/moderate optical depths throughout the volume of the emitting gas. Then the total number of the CO isotope molecules at the rotational level J is given by the expression

$$N_J = \frac{8\pi k \nu_{J,J-1}^2}{hc^3 A_{J,J-1}} \beta_{J,J-1}^{-1} L_{CO}(J, J-1), \quad (15)$$

where $A_{J,J-1}$ and $\beta_{J,J-1}$ are the Einstein coefficient and the escape probability of the $J \rightarrow J-1$ transition (e.g., Sobolev 1960; Castor 1970) respectively, and $L_{CO}(J, J-1)$ is the corresponding luminosity (Equation 13). A good approximation of the total H_2 mass is then provided by

$$M(H_2) = X_{CO} (N_1 + N_2 + N_3) \mu m_{H_2}, \quad (16)$$

where X_{CO} is the abundance of H_2 relative to the particular CO isotope and μm_{H_2} is the mean mass per H_2 molecule. Hence the expression for the X_{IS} factor that converts the $J=1-0$ luminosity of the CO isotope to molecular gas mass is as follows

$$X_{IS} = \frac{8\pi k \mu m_{H_2}}{hc^3} \left(\frac{\nu_{10}^2}{A_{10}} \right) \left[1 + \left(\frac{\nu_{21}}{\nu_{10}} \right)^2 \frac{A_{10}}{A_{21}} \frac{\beta_{10}}{\beta_{21}} r_{21} + \left(\frac{\nu_{32}}{\nu_{10}} \right)^2 \frac{A_{10}}{A_{32}} \frac{\beta_{10}}{\beta_{32}} r_{32} \right] \beta_{10}^{-1} X_{CO}, \quad (17)$$

where $r_{J+1, J} = L_{CO}(J+1, J)/L_{CO}(1, 0)$. After substitution this equation yields

$$X_{IS} = 0.078 [r] \left[1 + 0.42 \left(\frac{\beta_{10}}{\beta_{21}} \right) r_{21} + 0.26 \left(\frac{\beta_{10}}{\beta_{32}} \right) r_{32} \right] \beta_{10}^{-1}, \quad (18)$$

where we assumed $[H_2/^{12}CO] = 10^4$ and $[r] = [^{12}CO/x^{13}CO]$ is the abundance of ^{12}CO relative to the isotope used.

The assumption about the virialization of the average molecular cloud needed to deduce X (Equation 16) is no longer necessary. The omission of N_J for $J=0$ and $J > 3$ is not expected to have a major effect on the estimated $M(H_2)$ for the average conditions encountered in molecular clouds. This is suggested by a study of Giant Molecular

Cloud (GMC) cores done by Goldsmith et al. (1997), where they find good agreement between the virial mass and the mass deduced using this method and observations of the C¹⁸O isotope. They also find that the true mass can be at most ~ 2 times larger than the one computed from Equation 16. This occurs for cold ($T_{\text{kin}} \approx 10$ K) and diffuse ($n(H_2) < 10^3$ cm⁻³) gas where the term N_0 becomes important, or warm ($T_{\text{kin}} > 50$ K) and dense ($n(H_2) > 10^5$ cm⁻³) gas where levels above $J=3$ become significantly populated.

In the optically thin case, $\beta_{J,J-1} \sim 1$, and X_{IS} is independent of the details of the gas excitation conditions and velocity field that determine the value of $\beta_{J+1,J}$'s. Of course in the optically thick case these become important and more careful analysis is needed to estimate the escape probabilities.

Applying this method for ¹²CO or ¹³CO transitions, we find a gas mass of $M(H_2) \approx 5 \times 10^8 M_{\odot}$ from both isotopes. This value is $\sim 10 - 35$ times smaller than the one deduced from the standard galactic conversion factor X_G or its density/temperature “corrected” value X . Such a large discrepancy could not be due only to the fact that Equation 16 gives a lower limit to the molecular gas mass. Summing up the population of all the energy levels can result in a gas mass that is at most ~ 2 times larger (Goldsmith et al. 1997), which still leaves $M(H_2)$ at least ~ 5 times smaller than the one found from the standard galactic conversion factor.

Two effects that can contribute to this difference in the estimated gas mass are: a) the presence of a non-virialized gas component and, b) a large optical depth of the particular CO isotope used. The first effect will lead to an overestimate of the molecular gas mass whenever a factor that converts ¹²CO line luminosity to gas mass is used. Our analysis suggests that such a non-virialized molecular gas component indeed exists and dominates the ¹²CO emission in the central region of NGC 1068.

The second effect is due to the fact that in an optically thick medium significant

amounts of gas mass will contribute only a small fraction of the total observed luminosity. This is straightforward to understand when the line formation mechanism is local because then the observed emission comes from the outer layer of the cloud where $\tau \sim 1 - 3$ and a lot of gas mass can “hide” in its interior. The $\beta_{J+1,J}$ ’s factors can, to a certain extent, correct for this effect but obviously this correction becomes increasingly unreliable the larger the optical depth.

However in the case of large scale systematic motions within each cloud (and among the various clouds themselves), the various optically thick components appear centered at different velocities along the line profile and hence are “visible”. In such a situation significant gas mass can still “hide” provided that the more optically thick component has a lower temperature, a smaller velocity gradient and overall volume than the more diffuse gas component. This is exactly the type of molecular gas differentiation found for the gas in NGC 1068 and generally in starburst centers. A combination of a small spatial/velocity filling factor and a lower average temperature can reduce the luminosity contribution of the optically thick gas phase to $\lesssim 0.1\%$ of the luminosity of the diffuse, warmer gas component for equal amounts of gas mass.

The more accurate description of the molecular gas as a two-phase system allows a better estimate of the total gas mass as well as an estimate of the relative gas mass contained in each phase, namely

$$\frac{M_B}{M_A} = 0.13 (f_c \rho_{13}) \left[\frac{^{13}\text{CO}}{\text{C}^{18}\text{O}} \right] \frac{\left(T_{\text{kin}} e^{5.26/T_{\text{kin}}} \right) \beta_{10}^{-1}}{1 + 0.42 r_{21}^{(13)} + 0.26 r_{32}^{(13)}} R_{10}^{(18)}(B), \quad (19)$$

where T_{kin} and β_{10} are the average kinetic temperature and escape probability of C^{18}O $J=1-0$ in gas phase (B) and $r_{21}^{(13)}$ and $r_{32}^{(13)}$ are the line ratios for the optically thin ^{13}CO ($\beta_{J+1,J} \sim 1$, $J=0, 1, 2$) in phase (A).

Typical values from Table 3 yield $M_B/M_A \approx 5 - 10$ suggesting that most of the mass resides in the dense, optically thick gas phase (B). The estimated total gas mass is $M(H_2) = M_A + M_B \approx 3 \times 10^9 M_\odot$. As expected, this estimate yields a mass that is larger (by a factor of ~ 6) than the one found from Equation 18 under the assumption that ^{13}CO is optically thin throughout the emitting volume, yet smaller (by a factor of $\sim 2 - 6$) than the ones estimated from the standard galactic conversion factor.

5.6.1. *Estimates of $M(H_2)$ in starburst environments*

Our study of the IR-luminous starburst in NGC 1068 suggests that in the inner few kiloparsecs, the highly excited, non-virialized molecular gas component that dominates the ^{12}CO emission can be the cause of a systematic overestimate of molecular gas mass when a standard galactic conversion factor is used. In cases of other IR-luminous galaxies with powerful central starbursts like Mrk 231 and NGC 7469 the gas mass deduced from the standard galactic conversion factor is manifestly overestimated since it yields a mass that is comparable or larger than the dynamical mass contained within the same volume (Bryant & Scoville 1996; Genzel et al. 1995). While this can still be the result of a particular geometry of the CO-emitting gas (e.g., for Mrk 231, Bryant & Scoville 1996) it is also likely that the diffuse gas component in their starburst regions is in a highly excited state with high temperatures and large non-virial linewidths. In this case the velocity-integrated ^{12}CO $J=1-0$ luminosity will be significantly larger than in more quiescent environments, without this reflecting a proportionally larger molecular gas mass.

In the particular case of Seyferts, since type 2 are more likely to harbor starbursts than type 1 or field spirals (Maiolino et al. 1995), it follows that molecular gas mass deduced from their ^{12}CO $J=1-0$ luminosity will systematically overestimate their gas mass.

6. CONCLUSIONS

We conducted an extensive set of observations that map the distribution of the molecular gas in the inner $\sim 1' \times 1'$ of the archetypal Seyfert 2/starburst galaxy NGC 1068. The fully sampled maps of ^{12}CO , ^{13}CO $J=2-1$, $3-2$ transitions, a ^{12}CO $J=1-0$ map and two test spectra of the C^{18}O $J=2-1$ transition allowed us to probe the physical properties of the gas in great detail. Our main conclusions are the following:

1. A single-phase LVG model yields average conditions that correspond to relatively dense molecular gas ($\sim 10^4 \text{ cm}^{-3}$), with a temperature of $\sim 20 \text{ K}$ and optical depth $\tau \sim 1 - 2$ for the ^{12}CO $J=1-0$ transition. These conditions are not uniform and the ^{12}CO $r_{32} = (3-2)/(1-0)$ ratio (at resolution of $\sim 16''$) and earlier interferometric measurements of the $R_{10} = ^{12}\text{CO}/^{13}\text{CO}$ and $R_{10}^{(18)} = \text{C}^{18}\text{O}/^{13}\text{CO}$ $J=1-0$ ratios reveal a wide range of molecular gas properties in the inner $\sim 1' \times 1'$ starburst region of NGC 1068.
2. A single gas phase with moderate ^{12}CO $J=1-0$ optical depths cannot reproduce the high $\text{C}^{18}\text{O}/^{13}\text{CO}$ ($J=1-0$, $2-1$) intensity ratio and its large spatial variations observed in interferometric maps of the $J=1-0$ transition. A simple two-component model is used to describe the state of the “average” molecular cloud as consisting of a dense ($\gtrsim 10^4 \text{ cm}^{-3}$), more spatially concentrated component where C^{18}O $J=1-0$ has a moderate ($\tau \sim 1$) optical depth, surrounded by a more diffuse ($\sim 10^3 \text{ cm}^{-3}$), warmer gas phase where the ^{12}CO $J=1-0$ transition has $\tau \sim 1 - 2$.
3. The dense and more spatially concentrated phase contains most of the gas mass. Since the ^{13}CO in this phase is optically thick, using this isotope to deduce molecular gas mass under the assumption that it has small/moderate optical depth throughout the CO-emitting volume underestimates the true mass of this component and hence the total gas mass.

4. The diffuse gas phase dominates the observed ^{12}CO emission, it is highly excited and probably not virialized. This leads to an overestimate of molecular gas mass when the luminosity of the ^{12}CO $J=1-0$ line and a standard galactic conversion factor are used to deduce gas mass in starburst environments. Since type 2 Seyferts harbor starbursts more often than type 1 or field spirals, it follows that the use of the standard galactic conversion factor will systematically overestimate the global molecular gas mass in Seyfert 2's.

We would like to thank the great crew of telescope operators and support scientists at the James Clerk Maxwell Telescope where most of observations were taken. Special thanks must go to Per Friberg for his patient explanations of the telescope's workings and to Lorne Avery and Henry Matthews for performing some of the observations on our behalf. We are greatful to the referee Dr Tamara Helper for her suggestions that improved this work. Finally, we acknowledge the support of a research grant to E. R. S. from the Natural Sciences and Engineering Research Council of Canada.

This research has made use of the NASA/IPAC Extragalactic Database (NED), which is operated by the Jet Propulsion Laboratory, California Institute of Technology, under contract with the National Aeronautics and Space Administration.

REFERENCES

Aalto, S., Radford, S.J.E, Scoville, N. Z., & Sargent, A. I. 1997, ApJ, 475, L107

Aalto, S., Booth, R. S., Black, J. H., & Johansson, L. E. B. 1995, A&A, 300, 369

Bally, J., Stark, A. A., Wilson, R. W., & Henkel, C. 1988, ApJ, 324, 223

Barnes, J. E., & Hernquist, L. E. 1991, ApJ, 370, L65

Bergin, E. A., Snell, R. L., & Goldsmith, P. F. 1996, ApJ, 460, 343

Binney, J., Gerhard, O. E., Stark, A. A., Bally, J., & Uchida, K. I. 1991, MNRAS, 252, 210

Braine, J., & Combes, F. 1992, A&A, 264, 433

Bryant, P. M., & Scoville, N. Z. 1996, ApJ, 457, 678

Cameron, M., Genzel, R., & Storey, J. W. V., Experimental Astronomy, vol 3, pg 61

Casoli, F., Durpaz, C., & Combes, F. 1992, A&A, 264, 49

Castor, J. I. 1970, MNRAS, 149, 111

de Jong, T., Chu, S., & Dalgarno, A. 1975, ApJ, 199, 69

Devereux, N., Taniguchi, Y., Sanders, D. B., Nakai, N., & Young, J. S. 1994, AJ, 107 (6), 2006

Dickman R. L., Snell, R. L., & Schloerb, F. P. 1986, ApJ, 309, 326

Downes, D., Solomon, P. M., & Radford, S. J. E. 1993, ApJ, 414, L13

Eckart, A., Downes, D., Genzel, R., Harris, A. I., Jaffe, D. T., & Wild, W. 1990, ApJ, 348, 434

Eckart, A., Cameron, M., Jackson J. M., Genzel, R., & Harris, A. I. 1991, *ApJ*, 372, 67

Fuente, A., Martin-Pintado, J., Cernicharo, J., & Bachiller, R. 1993, *A&A*, 276, 473

Genzel, R., Weitzel, L. E., Tacconi-Garman, L. E., Blietz, M., Cameron, M., Krabbe, A., & Lutz, D. 1995, *ApJ* 444, 129

Goldsmith, P. F. 1972, *ApJ*, 176, 597

Goldsmith, P. F., & Langer, W. D. 1978, *ApJ*, 222, 881

Goldsmith, P. F., Bergin, E. A., & Lis, D. C. 1997, IAU Symposium No. 170, 113

Guesten, R. 1989, in: The physics and chemistry of interstellar molecular clouds - mm and sub-mm observations in astrophysics; Proceedings of the Symposium, Zermatt, Switzerland, Sept. 22-25, 1988 Berlin and New York, Springer-Verlag, p. 163-169.

Hasegawa, T. 1997, in CO: Twenty-five Years of Millimeter-wave Spectroscopy, IAU Symposium No. 170, pg 39

Heckman, T. M., Blitz, L., Wilson, A. S., Armus, L., & Miley, G. K. 1989, *ApJ*, 342, 735

Helfer, T. & Blitz, L. 1995, *ApJ*, 450, 90

Henkel, C., & Mauersberger, R. 1993, *A&A*, 274, 730

Henkel, C., Mauersberger, M., Wiklind, T., Hüttemeister, S., Lemme, C., & Millar, T. J. 1993, *A&A*, 268, L17

Irwin, J. A., & Avery, L. W. 1992, *ApJ*, 388, 328

Jackson, J. M., Paglione, A. D. T., Ishizuki, S., & Nguyen-Q-Rieu 1993, *ApJ*, 426, L77

Kaneko, N., Morita, K., Fukui, Y., Sugitani, K., Iwata, T., Nakai, N., Kaifu, N., & Liszt, H. S. 1989, *ApJ*, 337, 691

Knapp, G. R., Phillips, T. G., Huggins, P. J., Leighton, R. B., & Wannier, P. G. 1980, *ApJ*, 240, 60

Langer, W. D., & Penzias, A. A. 1993, *ApJ*, 408, 539

Lawrence, A., Rowan-Robinson, M., Leech, K., Jones, D. H. P., & Wall, J. V. 1989, *MNRAS*, 240, 329

Leung, C. M., & Liszt, H. S. 1976, *ApJ*, 208, 732

Maiolino, R., Ruiz, M., Rieke, G. H., & Keller, L. D. 1995, *ApJ*, 446, 561

Maiolino, R., Ruiz, M., Rieke, G. H., & Papadopoulos P. 1997, *ApJ*, 485, 552

Maloney, P., & Black, J. H. 1988, *ApJ*, 325, 389

Papadopoulos, P. P., Seaquist, E. R., & Scoville, N. Z. 1996, *ApJ*, 465, 173

Phillips, T. G., Knapp, G. R., Huggins, P. J., Werner, M. W., Wannier, P. G., Neugebauer, G., & Ennis, D. 1981, *ApJ*, 245, 512

Planesas, P., Gomez-Gonzalez J., & Martin-Pintado, J. 1989, *A&A*, 216, 1

Planesas, P., Scoville, N. Z., & Myers, S. T. 1991, *ApJ*, 369, 364

Radford, S. J. E., Solomon, P. M., & Downes, D. 1991, *ApJ*, 368, L15

Sage, L. J., Mauersberger, R., & Henkel, C. 1991, *A&A*, 249, 31

Sandage, A., & Tammann, G. A. 1981, Revised Shapley-Ames Catalog of Bright Galaxies (Washington: Carnegie Inst. of Washington)

Sanders, D. B., Soifer, B. T., Elias, J. H., Madore, B. F., Matthews, K., Neugebauer, G., & Scoville, N. Z. 1988, *ApJ*, 325, 74

Sanders, D. B., Scoville, N. Z., & Soifer, B. T. 1991, ApJ, 370, 158

Sanders, D. B., Scoville, N. Z., Tilanus, R. P. J., Wang, Z., & Zhou, S. 1993, in Back to the Galaxy, edited by F. Verter (Kluwer, Dordrecht), p. 311

Scoville, N. Z., & Good, J. C. 1989, ApJ, 339, 149

Sobolev, V. V. 1960, “Moving envelopes of stars” (Cambridge: Harvard University Press).

Solomon, P. M., & Barrett, J. W. 1991, in IAU Symp. 146, Dynamics of Galaxies and Molecular Cloud Distribution (Dordrecht: Kluwer), 235

Solomon, P. M., Downes, D., Radford, S. J. E., & Barrett, J. W. 1997, ApJ, 478, 144

Spergel, D. N., & Blitz, L. 1992, Nature, 357, 665

Stark, A. A., Bally, J., Wilson, R. W., Pound, M. W. 1989, In: *The Center of the Galaxy*, Morris M., (ed), Dordrecht. Kluwer, p. 129

Stark, A. A., Gerhard, O. E., Binney, J., & Bally, J. 1991 MNRAS, 248, 1P

Tacconi, L. J., Genzel, R., Blietz, M., Cameron, M., Harris, A. I., & Madden, S. 1994, ApJ, 426, L77

Telesco, C. M. 1988, ARA&A, 26, 343

Telesco, C. M., Becklin, E. E., Wynn-Williams, C. G., & Harper, D. A. 1984, ApJ, 282, 427

Thronson A. H. Jr., Walker, C. E., & Maloney, P. 1987, ApJ, 318, 645

Wall, W. F., & Jaffe, D. T. 1990, ApJ, 361, L45

Wall, W. F., Jaffe, D. T., Bash, F. N., Israel, F. P., Maloney, P. R., & Baas, F. 1993, ApJ, 414, 98

Wannier, P. G. 1980, *ARA&A*, 18, 399

Wild, W., Harris, A. I., Eckart, A., Genzel, R., Graf, U. U., Jackson, J. M., Russell, A. P. G., & Stutzki, J. 1992, *A&A*, 267, 447

Fig. 1.— The $\langle T_{mb} \rangle_{\Delta v}$ maps of ^{12}CO (top) and ^{13}CO (bottom) of the $J=2-1$ transition, with $\Delta v = 950 - 1300 \text{ km s}^{-1}$, at a resolution of $\theta_i = 24''$. For ^{12}CO the rms noise is $\sigma_{12} \approx 0.025 \text{ K}$, the contours are $(3, 5, 7, 9, 11, 13, 15, 17, 19, 21) \times \sigma_{12}$, and the greyscale range is $0.075-0.535 \text{ K}$. For ^{13}CO the rms noise is $\sigma_{13} \approx 0.003 \text{ K}$, the contours are $(3, 5, 7, 9, 11, 13, 15) \times \sigma_{13}$, and the greyscale range is $0.009-0.048 \text{ K}$.

Fig. 2.— The $\langle T_{mb} \rangle_{\Delta v}$ maps of ^{12}CO (top) and ^{13}CO (bottom) for the $J=3-2$ transition, with $\Delta v = 950 - 1300 \text{ km s}^{-1}$, at a resolution of $\theta_i = 16''$. For ^{12}CO the rms noise is $\sigma_{12} \approx 0.020 \text{ K}$, the contours are $(3, 5, 7, 9, 11, 13, 15, 17, 19, 21) \times \sigma_{12}$, and the greyscale range is $0.060-0.456 \text{ K}$. For ^{13}CO the rms noise is $\sigma_{13} \approx 0.002 \text{ K}$, the contours are $(3, 5, 7, 9, 11, 13) \times \sigma_{13}$, and the greyscale range is $0.006-0.026 \text{ K}$.

Fig. 3.— Channel maps of the ^{12}CO $J=3-2$ emission (contours) overlayed on the ^{12}CO $J=1-0$ emission (greyscale) at a common spatial resolution of $16''$ and velocity resolution of $\Delta v_{\text{chan}} \sim 8 \text{ km s}^{-1}$. The average rms noise of the ^{12}CO $J=3-2$ map is $\sigma_T(3-2) = 0.065 \text{ K}$, the lowest level contour is $3 \sigma_T(3-2)$ and the contour interval is $2 \sigma_T(3-2)$. The rms noise of the ^{12}CO $J=1-0$ map is $\sigma_T(1-0) = 0.08 \text{ K}$ and the greyscale range is: $0.25-2.50 \text{ K}$. The line ratio is estimated as $r_{32}^{(\text{chan})} = \langle T_{mb}(3-2) \rangle_{R_L} / \langle T_{mb}(1-0) \rangle_{R_L}$ for a radius of $R_L \lesssim 30''$ from the map center and it is reported at the bottom left corner of each channel map. The beam is shown at the bottom right corner of the first channel map.

Fig. 4.— Spectra of C^{18}O , ^{13}CO $J=2-1$ in two positions The offsets from the map center are the following A: $(\Delta a, \Delta \delta) = (8'', 0'')$, B: $(\Delta a, \Delta \delta) = (-8'', -3'')$

Fig. 5.— Area-averaged spectra of ^{12}CO , ^{13}CO for $J=3-2$, $2-1$, $1-0$, over a circular area with radius $R = 30''$.

Table 1
NGC 1068: The observations

Run	Receiver	Spectral line	Δv^c	θ_{HPBW}^d	$\Delta\theta_s^e$	Map size	
		$(T_{\text{sys}})^a$	$(\nu_0)^b$	$(\Delta v_{\text{chan}})^c$	$(\delta\theta_{\text{rms}})^d$	$(T_{\text{int}})^e$	$(\# \text{ of points})^f$
1994, Jan. 2-8	A2	^{12}CO J=2-1	900	21''	10''	$100'' \times 60''$	
1994, Nov. 26-29	(350-450)	(230.538)	(0.81)	(4'')	(1-2)		(85)
1994, Jan. 2-8	A2	^{13}CO J=2-1	941	21''	10''	$80'' \times 60''$	
1994, Nov. 26-29	(400-500)	(220.398)	(0.85)	(4'')	(10-20)		(57)
1997, Nov. 27	A2	C^{18}O J=2-1	945	22''
	(500)	(219.560)	(0.85)	(4'')	(90, 110)		(2)
1994, Nov. 26-29	B3i	^{12}CO J=3-2	600	14''	7''	$80'' \times 60''$	
1996, Jan. 16-28	(750-1000)	(345.795)	(0.54)	(3'')	(2)		(113)
1997, Nov. 27-Dec. 1	B3	^{13}CO J=3-2	900	14''	7''	$60'' \times 50''$	
1997, Dec. 27-29	(400-500)	(330.588)	(0.57)	(3'')	(10-15)		(87)

^a Typical system temperatures for the corresponding receiver in Kelvin.

^b The rest frequency of the spectral line in GHz.

^c The corresponding velocity range Δv , and resolution Δv_{chan} in km s⁻¹.

^d The HPBW of the gaussian beam, and the rms pointing error $\delta\theta_{\text{rms}}$.

^e The sampling interval $\Delta\theta_s$, and the integration time T_{int} per point in minutes.

^f The number of points corresponding to each map.

Table 2
NGC 1068: The global line ratios

$\frac{^{12}\text{CO}(3-2)}{^{12}\text{CO}(1-0)}$ (r ₃₂)	$\frac{^{12}\text{CO}(2-1)}{^{12}\text{CO}(1-0)}$ (r ₂₁)	$\frac{^{12}\text{CO}(3-2)}{^{13}\text{CO}(3-2)}$ (R ₃₂)	$\frac{^{12}\text{CO}(2-1)}{^{13}\text{CO}(2-1)}$ (R ₂₁)	$\frac{^{12}\text{CO}(1-0)}{^{13}\text{CO}(1-0)}$ (R ₁₀)	$\frac{^{13}\text{CO}(1-0)}{^{13}\text{CO}(1-0)}$ (R ₁₀ ⁽¹⁸⁾)	$\frac{^{13}\text{CO}(2-1)}{^{13}\text{CO}(2-1)}$ (R ₂₁ ⁽¹⁸⁾)
0.52 ± 0.17	0.68 ± 0.23	14 ± 3	10 ± 2	14 ± 2 ^a	0.30 ± 0.10 ^b	0.23 ± 0.04 ^c

^a OVRO measurement (Papadopoulos, Seaquist & Scoville 1996), Young & Sanders (1986).

^b OVRO measurement (Papadopoulos, Seaquist & Scoville 1996).

^c The average of the two values measured with the JCMT.

Table 3
NGC 1068: Two-phase model

Gas phase (B) ^a $\tau_{10}^{(18)}$, $f_c \rho_{13}$, T_{kin}	Line ratios (A) ^b $r_{21}, r_{32}, R_{10}, R_{21}, R_{32}$	LVG parameters (A) ^c $T_{\text{kin}}, n(H_2), \Lambda$	Excitation (A) ^d $E_{10}^{(13)}, \tau_{10}^{(12)}$
0.5, 1.35, 15	0.97, 0.74, 32, 15, 31 (1.18, 0.73, 27, 23, 31)	35, 3×10^3 , 1×10^{-6} $\chi^2 = 3.2$	3.8, 0.29
0.7, 0.70, 10	0.97, 0.74, 23, 13, 20 (1.05, 0.76, 17, 13, 20)	35, 3×10^3 , 3×10^{-6} $\chi^2 = 3.2$	2.8, 0.94
0.9, 0.50, 15	0.97, 0.74, 20, 12, 20 (1.05, 0.76, 17, 13, 20)	35, 3×10^3 , 3×10^{-6} $\chi^2 = 0.95$	2.8, 0.94
1.1, 0.40, 20	0.97, 0.74, 19, 12, 20 (1.05, 0.76, 17, 13, 20)	35, 3×10^3 , 3×10^{-6} $\chi^2 = 0.53$	2.8, 0.94
1.5, 0.30, 20-40	0.97, 0.76, 18, 12, 19 (1.05, 0.76, 17, 13, 20)	35, 3×10^3 , 3×10^{-6} $\chi^2 = 0.37 - 0.45$	2.8, 0.94
2.5, 0.25, 15-40	0.97, 0.74, 17, 11, 17-18 (1.05, 0.76, 17, 13, 20)	35, 3×10^3 , 3×10^{-6} $\chi^2 = 1.2 - 0.8$	2.8, 0.94

^a The physical conditions of the gas in phase (B): $\tau_{10}^{(18)}$ is the optical depth of the C^{18}O $J=1-0$ transition, T_{kin} is the kinetic temperature and $f_c \rho_{13}$ is defined in Equation (3).

^b The line ratios estimated for gas phase (A), the ones in the parenthesis are the values obtained from the LVG model with the minimum χ^2 , where $\chi^2 = \sum_i \frac{1}{\sigma_i^2} [R_{(i)} - R_{\text{obs}}]^2$ and $R_{(i)}$, R_{obs} are the model and observed line ratios respectively, with σ_i being the corresponding 1σ uncertainty.

^c The LVG parameters (see text) corresponding to the best fit of the line ratios of gas phase (A).

^d $E_{10}^{(13)} = T_{\text{exc}}/T_{\text{kin}}$ for ^{13}CO $J=1-0$ and $\tau_{10}^{(12)}$ is the optical depth of the ^{12}CO $J=1-0$ transition for gas phase (A).

This figure "fig1.gif" is available in "gif" format from:

<http://arxiv.org/ps/astro-ph/9901394v1>

This figure "fig2.gif" is available in "gif" format from:

<http://arxiv.org/ps/astro-ph/9901394v1>

This figure "fig3.gif" is available in "gif" format from:

<http://arxiv.org/ps/astro-ph/9901394v1>

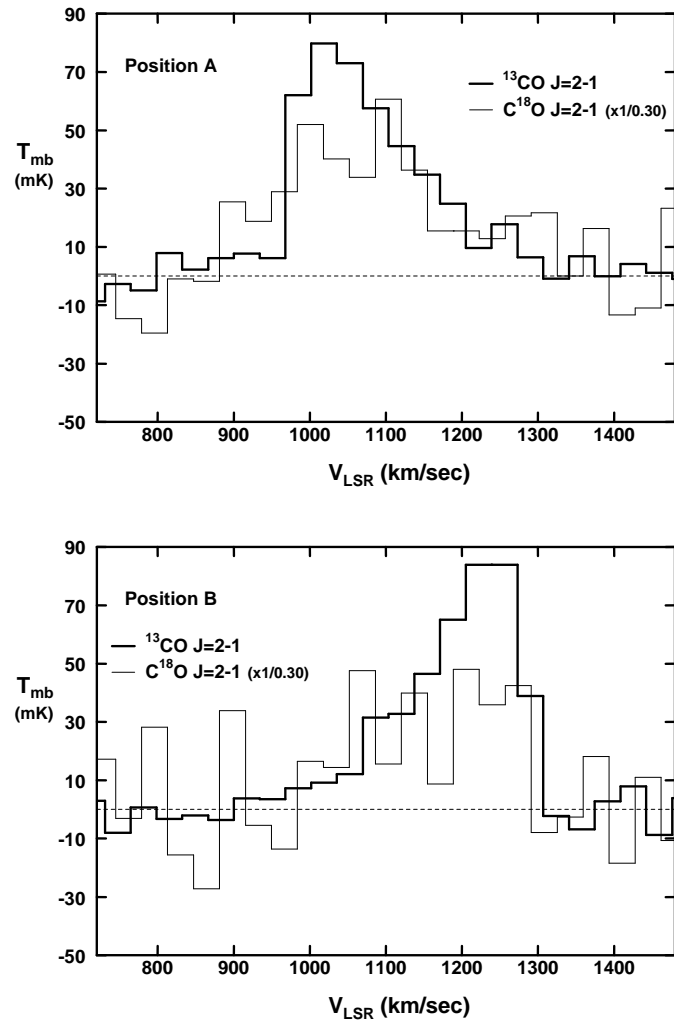


Figure 4

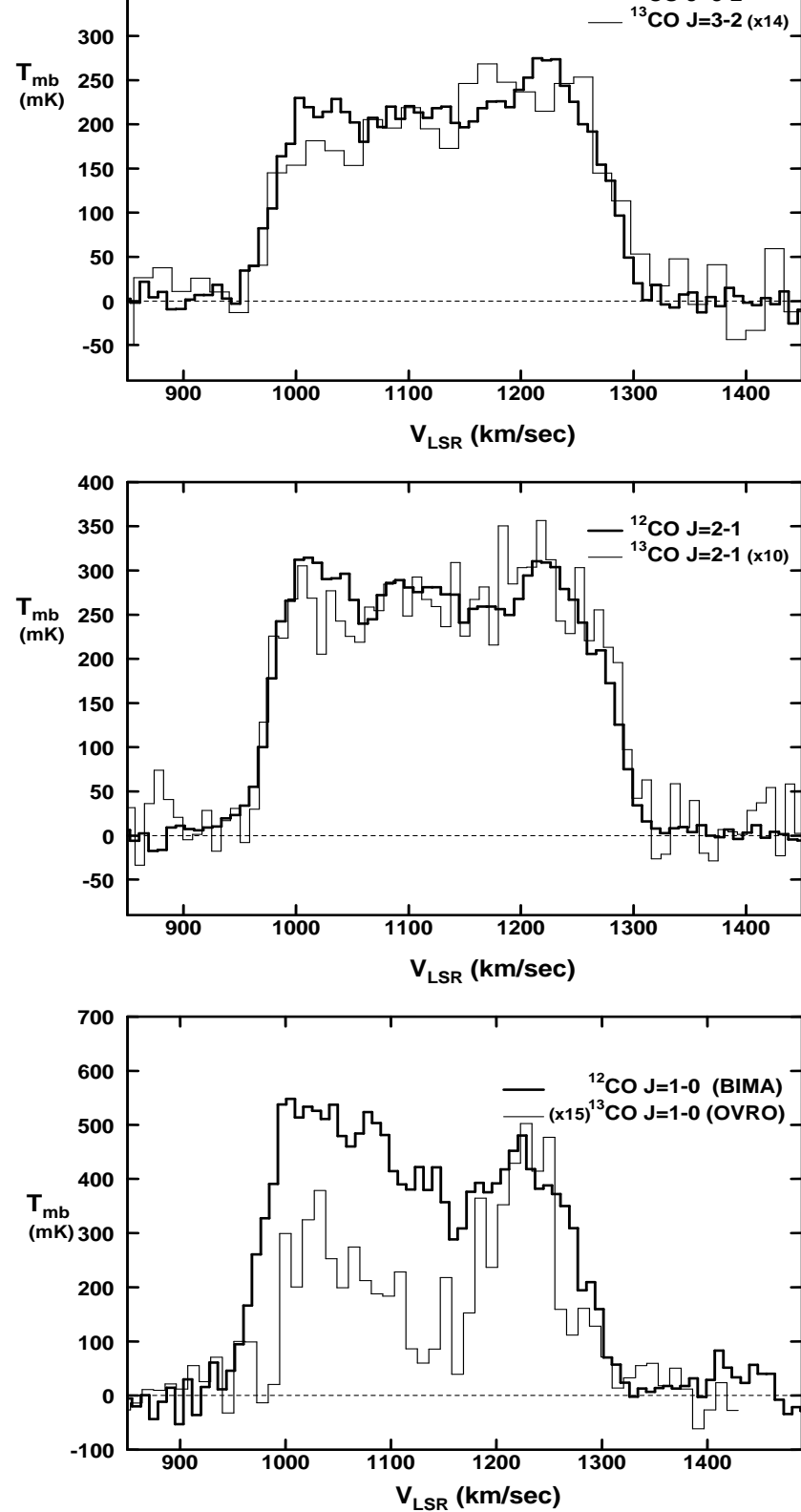


Figure 5